HEATING OF IONS BY LOW-FREQUENCY ALFVÉN WAVES IN SOLAR ATMOSPHERE

A Thesis
Presented to
The Academic Faculty

by

Chuanfei Dong

In Partial Fulfillment
of the Requirements for the Degree
Master of Science in the
School of Earth and Atmospheric Sciences

Georgia Institute of Technology
December 2010

HEATING OF IONS BY LOW-FREQUENCY ALFVÉN WAVES IN SOLAR ATMOSPHERE

Approved by:

Professor Carol Paty, Committee Chair
School of Earth and Atmospheric Sciences
Georgia Institute of Technology

Professor Carol Paty, Advisor
School of Earth and Atmospheric Sciences
Georgia Institute of Technology

Professor Josef Dufek
School of Earth and Atmospheric Sciences
Georgia Institute of Technology

Professor Zhigang Peng
School of Earth and Atmospheric Sciences
Georgia Institute of Technology

Date Approved: 15 November 2010

To my family, for their encouraging and believing in me. For my grandma who brought me up and taught me how to be a person with high morality. For my girlfriend, who always helps me whatever I ask for.

ACKNOWLEDGEMENTS

First, I want to thank my advisor Prof. Carol Paty, who is a very nice person. She actually is also one of my good friends. She helps me not only in my academic study but also in my daily life. Second, I want to thank my committee members, Prof. Josef Dufek, Prof. Zhigang Peng, who contributed a lot of their time to improve my thesis. Third, I want to thank my friends, Xiaofeng Meng, Joe Estep, Lujia Feng, Molly Lindle, Mary Benage, Yan Luo, Chunquan Wu, Ozge Karakas and so on. I really have a nice time with them. Finally, I want to thank my family and my girlfriend Nan Liu for their patience and support.

TABLE OF CONTENTS

LIST OF TABLES

LIST OF FIGURES

CHAPTER I

INTRODUCTION

1.1 Structure of the Sun and its atmosphere

The Sun is the star at the center of our solar system, and in some ways it can viewed as a natural plasma laboratory. Fig.1 illustrates the structure of the sun and its atmosphere. We can divide the sun to four main regions: core, radiative zone, convective zone, and photosphere. The solar atmosphere comprises five principal zones: the temperature minimum, the chromosphere, the transition region, the corona, and the heliosphere. We will briefly introduce them one by one.

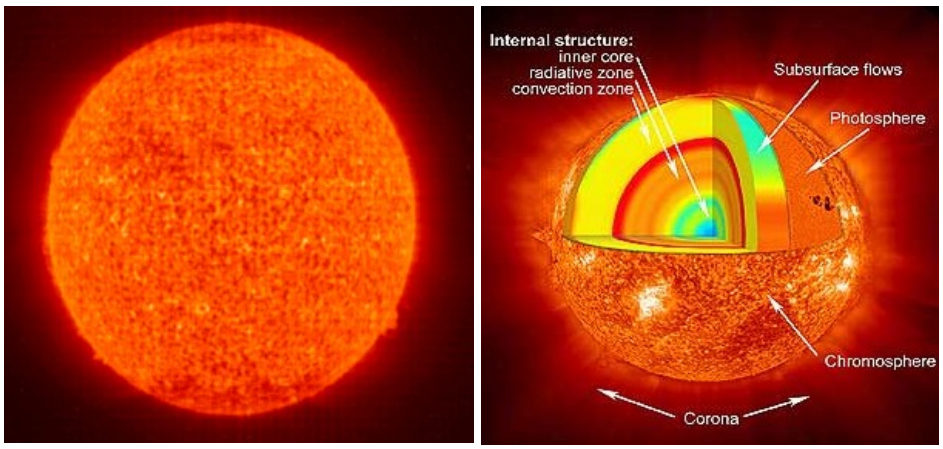

Figure 1: The Structure of the Sun and its atmosphere (Image Credit: NASA).

Core: The core of the sun is considered to extend from the center to about 0.2 to 0.25 of solar radii [1]. It has a density of up to $1.5\times10^5\ kg/m^3$ [2] and a temperature

of close to 13,600,000 K. The core is the only location in the Sun that produces an appreciable amount of heat through fusion; inside 0.24 solar radii, 99% of the power has been generated, and by 0.3 solar radii, fusion has stopped nearly entirely [3].

Radiative zone: From about 0.25 to about 0.7 solar radii, solar material is hot and dense enough that thermal radiation is sufficient to transfer the intense heat of the core outward [5].

Convective zone: In the Sun's outer layer, from its surface down to approximately 200,000 km (or the outer 0.3 solar radii), the solar plasma is not dense enough or hot enough to transfer the heat energy of the interior outward through radiation [**?**]. In this region, convection provides the dominant mechanism for energy transport.

Photosphere: The visible surface of the Sun, the photosphere, is the layer below which the Sun becomes opaque to visible light. The Sun's photosphere has a temperature between 4500 and 6000 K [6] and a density of about 2×10^4 kg/m^3 [7].

The temperature minimum: The coolest layer of the Sun is a temperature minimum region about 500 km above the photosphere, with a temperature of about 4,100 K [8].

Chromosphere: A layer above the temperature minimum layer, the chromosphere is about 2,000 km thick, dominated by a spectrum of emission and absorption lines [8]. The temperature in the chromosphere increases gradually with altitude, ranging up to around 20,000 K near the top [8].

Transition region: Above the chromosphere there is a thin (about 200 km) transition region in which the temperature rises rapidly from around 20,000 K in the upper chromosphere to coronal temperatures closer to 1,000,000 K [9].

Corona: The corona is the extended outer atmosphere of the sun, which is much larger in volume than the sun itself. The corona continuously expands into the space forming the solar wind, which fills all the solar system. The low corona, which is very near the surface of the Sun, has a particle density around $10^{15} \sim 10^{16}$ m^{-3} [10]. The

Solar Region	Photosphere	Chromosphere	Corona
Location	surface of the sun ($\sim$ 1 solar radius)	above the photosphere, roughly 2,000 km deep	above the chromosphere, extending millions of kilometers into space
Temperature	4500$\sim$6000 K	20,000 K	1,000,000$\sim$2,000,000 K (average) 8,000,000$\sim$ 20,000,000 K (hottest)

Table 1: The locations and temperature of three most popular solar regions that space physicists focus on.

average temperature of the corona and solar wind is about 1,000,000$\sim$2,000,000 K; however, in the hottest regions it is 8,000,000$\sim$20,000,000 K [9].

Heliosphere: The heliosphere, which is the cavity around the sun filled with the solar wind plasma, extends from approximately 20 solar radii (0.1 AU) to the outer fringes of the solar system ($\sim$ 94 AU) [11], where it encounters the interstellar wind.

1.2 Alfvén wave and its dispersion relation

In ideal Magnetohydrodynamics (MHD) the motion of the plasma parallel to magnetic field-lines is associated with the dynamics of sound waves, whereas the motion perpendicular to field-lines is associated with the dynamics of Alfvén waves. Alfvén waves involve the "twanging" motion of magnetic field-lines—a bit like the twanging of guitar strings as shown in Fig.2. Due to the "frozen-in" effect, which means that the magnetic field and the plasma are bound together via the Lorentz force. We can describe that each magnetic field line as having a "mass". Thus a magnetic field line with a unit length has a mass of $\varrho = \rho_0/B_0$, and the corresponding tension is $T = B_0/\mu$ (μ is the permeability of free space). Then we can get the Alfvén speed (the speed that Alfvén waves propagating through the magnetized plasmas) as follows:

$$v_A = \sqrt{\frac{T}{\varrho}} = \sqrt{\frac{B_0/\mu}{\rho_0/B_0}} = \sqrt{\frac{B_0^2}{\mu\rho_0}} \tag{1}$$

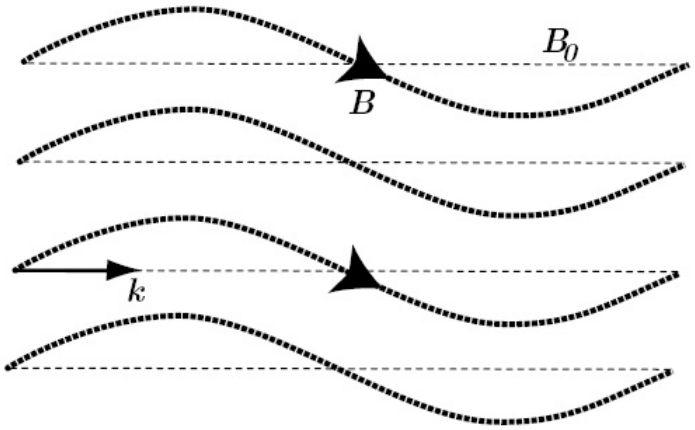

Figure 2: Magnetic field perturbation associated with a shear-Alfvén wave.

Dispersion often refers to frequency-dependent effects in wave propagation. The dispersion relation is very important since it describes the interrelations of wave properties like wavelength, frequency, velocities, refraction index, attenuation coefficient. In the following paragraphs, we will derive the dispersion relation of Alfvén wave based on the ideal MHD equations:

$$\rho\frac{d\mathbf{u}}{dt} = \mathbf{J}\times\mathbf{B} \quad (Momentum\ conservation) \tag{2}$$

$$\mathbf{J} = \frac{1}{\mu}\bigtriangledown\times\mathbf{B} \quad (Ampere's\ circuital\ law) \tag{3}$$

$$\bigtriangledown\cdot\mathbf{B} = \mathbf{0} \quad (Gauss's\ law\ for\ magnetism) \tag{4}$$

$$\bigtriangledown\times\mathbf{E} = -\frac{\partial\mathbf{B}}{\partial t} \quad (Maxwell - Faraday\ equation) \tag{5}$$

$$\mathbf{E}+\mathbf{u}\times\mathbf{B} = 0 \quad (Generalized\ Ohm's\ law\ for\ nonresistance) \tag{6}$$

where $\mathbf{u}$ is the particle (ion and electron) velocity, $\mathbf{B}$ is the magnetic filed vector, $\mathbf{E}$ is the electric filed vector, ρ is the mass density, $\mathbf{J}$ is total current density and μ is

the permeability of free space. Since we are concerned with small departures from equilibrium we can apply perturbation theory to the ideal MHD equations above [12]. We write

$$\rho(\mathbf{r},t) = \rho_0(\mathbf{r})+\rho_1(\mathbf{r},t) \tag{7}$$

$$\mathbf{u}(\mathbf{r},t) = \mathbf{u}_0(\mathbf{r})+\mathbf{u}_1(\mathbf{r},t) \tag{8}$$

$$\mathbf{B}(\mathbf{r},t) = \mathbf{B}_0(\mathbf{r})+\mathbf{B}_1(\mathbf{r},t) \tag{9}$$

$$\mathbf{E}(\mathbf{r},t) = \mathbf{E}_0(\mathbf{r})+\mathbf{E}_1(\mathbf{r},t) \tag{10}$$

$$\mathbf{J}(\mathbf{r},t) = \mathbf{J}_0(\mathbf{r})+\mathbf{J}_1(\mathbf{r},t) \tag{11}$$

where the subscripts 0 and 1 denote equilibrium and perturbation values, respectively. We assume there is no electric field and the magnetic file line is static initially, thus no total current density (see Eq.(3)). Therefore, we can assume the equilibrium states as follows:

$$\mathbf{u}_0 = 0,\ \mathbf{J}_0 = 0,\ \mathbf{E}_0 = 0,\ \mathbf{B}_0 = B_0\mathbf{e}_z,\ \rho_0 = \rho_0 \tag{12}$$

where B_0 and ρ_0 are constant. Now substituting Eq.(3) into Eq.(2) for current density $\mathbf{J}$, we get

$$\rho_0\frac{\partial \mathbf{u}_1}{\partial t} = \frac{1}{\mu}(\bigtriangledown \times \mathbf{B}) \times \mathbf{B} = \frac{1}{\mu} \bigtriangledown \cdot(\mathbf{BB}-\frac{1}{2}B^2\overleftrightarrow{I}) \tag{13}$$

We assume $\mathbf{B}_1 = B_1\mathbf{e}_y$ as show in Fig.3. Since $\mathbf{B}_1$ is the turbulence magnetic field and $\mathbf{u}_1$ is corresponding turbulence velocity, $\mathbf{u}_1 \parallel \mathbf{B}_1$. Thus two terms in the right

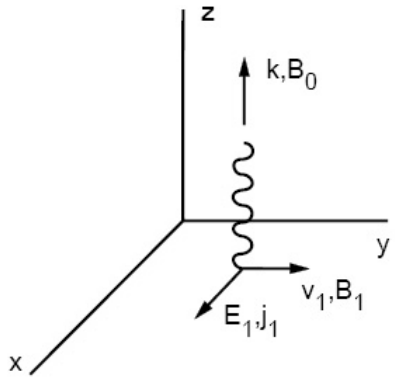

Figure 3: Geometry of a linearly polarized Alfvén wave.

hand of the Eq.(13) above can be approximated to the first order as

$$B^2 = (B_0\mathbf{e}_z + B_1\mathbf{e}_y)(B_0\mathbf{e}_z + B_1\mathbf{e}_y) \approx B_0^2, \;\Rightarrow\; \bigtriangledown\cdot(B^2\overleftrightarrow{I}) = 0 \tag{14}$$

where $\overleftrightarrow{I}$ is the unit tensor,

$$\bigtriangledown\cdot(\mathbf{BB}) = (\bigtriangledown\cdot\mathbf{B})\mathbf{B} + (\mathbf{B}\cdot\bigtriangledown)\mathbf{B} = (\mathbf{B}_0\cdot\bigtriangledown)\mathbf{B}_1 = B_0\frac{\partial B_1}{\partial z}\mathbf{e}_y. \tag{15}$$

From substituting into Eq.(13), we get

$$\rho_0\frac{\partial u_1}{\partial t}\mathbf{e}_y = \frac{B_0}{\mu}\frac{\partial B_1}{\partial z}\mathbf{e}_y \Rightarrow \rho_0\frac{\partial u_1}{\partial t} = \frac{B_0}{\mu}\frac{\partial B_1}{\partial z} \tag{16}$$

$$\frac{\partial E_1}{\partial z}\mathbf{e}_y = -\frac{\partial B_1}{\partial t}\mathbf{e}_y \Rightarrow \frac{\partial E_1}{\partial z} = -\frac{\partial B_1}{\partial t} \tag{17}$$

$$E_1\mathbf{e}_x + u_1B_0\mathbf{e}_x = 0 \;\Rightarrow\; E_1 + u_1B_0 = 0 \tag{18}$$

where we use the linearizing Faraday's law and generalized Ohm's law

$$\bigtriangledown\times\mathbf{E}_1 = -\frac{\partial\mathbf{B}_1}{\partial t} \tag{19}$$

$$\mathbf{E}_1 + \mathbf{u}_1\times\mathbf{B}_1 = 0 \tag{20}$$

thus we know $\mathbf{E}_1 = E_1\mathbf{e}_x$ are necessarily in the direction of $\mathbf{e}_x$. Using Fourier transform, Eqs.(16-18) are reduced to

$$-\omega\rho_0 u_k = \frac{B_0}{\mu} k B_k \tag{21}$$

$$kE_k = \omega B_k \tag{22}$$

$$E_k = -B_0 u_k \tag{23}$$

Finally we get the dispersion relation of Alfvén wave

$$\omega = k v_A, v_A = \sqrt{\frac{B_0^2}{\mu\rho_0}} \tag{24}$$

where $v_A = \sqrt{\frac{B_0^2}{\mu\rho_0}}$ is the shear Alfvén wave speed.

1.3 Previous studies

The chromosphere, the region between the solar surface and the corona, is permeated by low-frequency Alfvén waves with strong amplitudes [13] while the plasma beta value in this region is low [13, 14]. Also, in situ observations find that in interplanetary space the Alfvén wave magnetic field amplitude δB_w is often comparable to the ambient magnetic field intensity B_0 such that it is common to find $\delta B_w/B_0$ on the order of 0.3-0.5 [15]. In some case it may even reach 0.8 [16]. The chromospheric and coronal plasmas are much hotter than the visible photosphere as shown in Section 1.1. The heating mechanisms in these regions, however, have not yet been fully understood [17, 18]. Alfvén waves have long been considered to play a crucial role in heating of plasma in these two regions and in magnetic fusion devices [13, 18–22]. Numerous theoretical and experimental papers have been published to investigate resonant heating of ions by Alfvén waves [23–26]. In these works, the cyclotron resonant condition is necessary for ion heating by the Alfvén waves, and in general the frequencies of the applied Alfvén waves are comparable to the cyclotron frequency.

However, the heating of ions by low-frequency Alfvén waves and related problems have triggered great interest in recent years [13, 27–38]. Here the ions can be heated by Alfvén waves via nonresonant interactions, which means $\omega \ll \Omega_q$, where ω is the frequency of the Alfvén waves and Ω_q denotes the gyrofrequency for ion species labeled q. Among these works, various simulation and theoretical methods, such as test particle approach with analytic solutions [28, 30, 32, 33, 37, 38], hybrid simulations [27,35,36], and kinetic theory [31,35,36], have been used to validate the heating mechanism by low-frequency Alfvén wave interactions. Furthermore, all these works required the plasma beta value to be low and the relative amplitude ($\delta B_w/B_0$) of the Alfvén wave between 0.2 and 0.35 (thus the relative energy density ${\delta B_w}^2/{B_0}^2$ ranges from 0.04 to 0.12). Evidence of ion heating by low-frequency Alfvén waves has also been found in laboratory experiments [39–41].

Recently, Leake *et al.* [42] numerically demonstrate that Alfvén waves can propagate through the partially ionized solar chromosphere. They find that Alfvén waves with frequencies below 0.01 Hz are unaffected by the collisions between the ions and neutrals, and that waves with frequencies below 0.6 Hz will not be completely damped. This finding is interesting since previous works [43, 44] indicate that when Alfvén waves propagate in partially ionized plasmas, a slippage between the ion and neutral populations will lead to dissipation of the waves.

In the following sections, we demonstrate that the low-frequency Alfvén waves propagating along the background magnetic field $\mathbf{B}_0 = B_0\mathbf{i}_z$, can heat ions even in partially ionized plasmas (chromosphere). We also examine the heating caused by obliquely propagating Alfvén waves in fully ionized plasmas (corona). It is important to note the heating mechanism in this work is different from the previous research [29, 42]. The heating process in the present work is due to a randomization of the spatial velocity distribution in the ion population, which is caused by the nonresonant Alfvén wave interactions. For the partially ionized situation, we find that the heating process

becomes less efficient than the situation with no ion-neutral collisions. Moreover, the heating process is only effective for low-beta plasmas and Alfvén wave frequencies lower than 0.6 Hz; the most efficient heating occurs when $\omega \leq 0.01$ Hz since the waves are not damped as shown in the previous paragraph. For ion heating by obliquely propagating Alfvén waves in fully ionized plasmas, we find the heating process to be more efficient than the situation with Alfvén waves propagating along the background magnetic field. The heating efficiency depends on the angle between wave propagating and ambient magnetic field. Another interesting finding is that the parallel kinetic temperature can become even larger than the perpendicular component which is also different from the results under Alfvén waves propagating along the background magnetic field.

CHAPTER II

HEATING OF IONS BY LOW-FREQUENCY ALFVÉN WAVES IN PARTIALLY IONIZED PLASMAS

We consider the Alfvén waves have a spectrum and the dispersion relation can be described as $\omega = kv_A$ (v_A is the Alfvén speed, ω and k are the wave angular frequency and wave number, respectively). This relationship is still appropriate even when the plasma is partially ionized, as described in the following paragraphs. Without loss of generality, we consider left-hand circular polarization in this chapter. The wave magnetic field vector $\delta\mathbf{B}_w$ and electric field vector $\delta\mathbf{E}_w$ can be expressed as

$$\delta\mathbf{B}_w = \sum_k B_k(\cos\phi_k \mathbf{i}_x - \sin\phi_k \mathbf{i}_y), \tag{25}$$

$$\delta\mathbf{E}_w = -\frac{v_A}{c}\mathbf{b}\times\delta\mathbf{B}_w, \quad \mathbf{b} = \frac{\mathbf{B}_0}{B_0} \tag{26}$$

where $\mathbf{i}_x$ and $\mathbf{i}_y$ are unit directional vectors, $\phi_k = k(v_A t - z) + \varphi_k$ denotes the wave phase and φ_k is the random phase for mode k. In the following, we pay attention to the protons only, whose equation of motion is described by

$$m_i\frac{d\mathbf{v}}{dt} = q_i\left(\delta\mathbf{E}_w + \frac{\mathbf{v}}{c}\times(\mathbf{B}_0 + \delta\mathbf{B}_w)\right) + m_i\nu_{in}(\mathbf{u}-\mathbf{v}), \quad \frac{d\mathbf{r}}{dt} = \mathbf{v} \tag{27}$$

where $\mathbf{v}$ is the ion velocity, $\mathbf{u}$ is the bulk velocity of a background neutral fluid, and ν_{in} is the frequency for elastic collisions between ions and neutrals. The collision frequency responsible for momentum transfer between species i and n is defined as:

$$\nu_{in} = \frac{m_n}{m_i + m_n} n_n \sqrt{\frac{8k_B T}{\pi m_{in}}}\sigma_{in}, \tag{28}$$

with $m_{in} = (m_i m_n)/(m_i + m_n), \sigma_{in}$ the collisional cross-section for collisions between the two species. Here $m_i = m_n$ because the plasma we studied in this chapter is

assumed to be entirely composed of hydrogen which leads to $m_{in} = m_i/2$. The wave phase speed v_{ph} here is defined by [43]:

$$v_{ph} = \frac{\omega}{k} = v_A \sqrt{1 - i\frac{\rho_n}{\rho_{tot}}\frac{\omega}{\nu_{ni}}} \tag{29}$$

in which ρ_n is the mass density of neutrals, ρ_{tot} is the total mass density of the plasma, and ν_{ni} is neutral-ion collision frequency. Therefore, the relationship $\rho_n/\rho_{tot} < 1$ is necessarily valid. As shown by De Pontieu and Haerendel, for waves with $\nu \leq 1$ Hz, the assumption $\omega \ll \nu_{ni}$ ($\omega/\nu_{ni} \ll 1$) holds throughout the chromosphere [43]. Furthermore, most theories for the generation of Alfvén waves in the solar atmosphere predict typical frequencies below 1 Hz [43], which has also been observed by the Japanese Hinode satellite [13]. These allow us to simplify Eq.(29) to

$$v_{ph} = \frac{\omega}{k} = v_A \sqrt{1 - i\frac{\rho_n}{\rho_{tot}}\frac{\omega}{\nu_{ni}}} \approx v_A \tag{30}$$

Hence the relationship $\omega = kv_A$ is still appropriate.

Defining $v_\perp = v_x + iv_y$, $u_\perp = u_a + iu_b$, $v_\parallel = v_z$, $u_\parallel = u_c$ (here subscript a, b and c can be x, y or z) and $\delta B_\omega = \sum_k B_k e^{-i\phi_k}$; we are left with

$$\frac{dv_\perp}{dt} + (i\Omega_0 + \nu_{in})v_\perp = i(v_\parallel - v_A)\sum_k \Omega_k e^{-i\phi_k} + \nu_{in}u_\perp \tag{31}$$

$$\begin{aligned} \frac{dv_\parallel}{dt} &= -v_x \sum_k \Omega_k \sin\phi_k - v_y \sum_k \Omega_k \cos\phi_k + \nu_{in}(u_\parallel - v_\parallel) \\ &= -Im(v_\perp \sum_k \Omega_k e^{i\phi_k}) + \nu_{in}(u_\parallel - v_\parallel), \quad \frac{dz}{dt} = v_\parallel \end{aligned} \tag{32}$$

where $\Omega_0 = \frac{q_i B_0}{m_i c}$ (the proton gyrofrequency), $\Omega_k = \frac{q_i B_k}{m_i c}$. $Im(\ )$ denotes the imaginary part of its argument. As a first-order approximation, we can assume $v_\parallel \approx v_\parallel(0)$, where $v_\parallel(0)$ is the particle's initial parallel velocity. The approximation is valid when $\frac{\Omega_k}{\Omega_0} = \frac{B_k}{B_0}$ is small enough and the frequencies of the Alfvén wave are sufficiently low to ensure that $\mid \Omega_0 \mid \gg \mid k\left(v_\parallel(0) - v_A\right) \mid$. For simplicity, we assume the bulk velocities of the cold neutrals $u_x(t) = u_y(t) = u_z(t) \approx 0$ and ion-neutral collision frequency

$\nu_{in} \approx constant$, which provides a lower limit for the amount of ion heating. Since the ions and background neutral fluid are both "cold" initially, it is reasonable to assume $\mathbf{u}(t) \approx 0$ due to the relatively short time scales considered in this chapter and the high neutral fraction (detailed below).

The ion-neutral collision frequency used in this chapter is based on the VAL C model of the quiet Sun [45], where we select two values of the ratio a (the ratio of ion-neutral collision frequency to ion gyrofrequency), 0.1 and 0.5, to represent the partially ionized chromosphere. According to VAL C model [45], when $a = \nu_{in}/\Omega_0 \geq 0.05$, the ratio of neutral density to ion density $\lambda = n_n/n_i \gg 1$, which indicates that the amount of neutrals is much larger than that of ions. It is important to note that although the value of ratio $\lambda \gg 1$ indicates that ν_{in} is large (see Eq.(28)), the value of Ω_0 can also be large due to the background magnetic field B_0 ($\Omega_0 = \frac{q_i B_0}{m_i c}$), thus the value of ratio a can still be very small.

In the following, we focus on the perpendicular velocity component due to the fact that the ion temperature increase is more prominent along the perpendicular direction than the parallel direction [30, 32]. We acknowledge that the anisotropy between $v_\perp$ and $v_\parallel$ should be alleviated after a sufficiently long period of time due to the collisional effects, however, this is not taken into account due to the relatively short time scales considered in this chapter. Even over much longer timescales, where ions temperatures become isotropic, the fact that the ions will be heated by Alfvén waves remains unchanged. With the initial condition $v_\perp = v_\perp(0)$ and $z = z(0)$, the solution of Eq.(49) can be written as:

$$\begin{aligned} v_\perp &= v_\perp(0)e^{-(i\Omega_0+\nu_{in})t} + \frac{\nu_{in}u_\perp(\nu_{in}-i\Omega_0)}{{\Omega_0}^2+{\nu_{in}}^2}\left[1-e^{-i\Omega_0 t}e^{-\nu_{in}}\right] \\ &- \frac{\sum_k \Omega_k\left[v_A - v_\parallel(0)\right](\Omega_0+i\nu_{in})}{{\Omega_0}^2+{\nu_{in}}^2}\left[e^{-ik(v_A t-z)-i\varphi_k} - e^{i(kz(0)-\varphi_k)}e^{-(i\Omega_0+\nu_{in})t}\right] \end{aligned} \quad (33)$$

Here, we use the approximations that $\Omega_0 - k[v_A - v_\parallel(0)] \approx \Omega_0$ and $z = z(0) + v_\parallel(0)t$. We can see from the solution that the ion-neutral frequency ν_{in} has a negative effect

on the heating process because of the term $e^{-\nu_{in}t}$. In order to verify that the analytical solution is correct, we set $\nu_{in} = 0$. Then the Eqs. (39, 49, 50) are reduced to those found in previous work [28, 30, 32] where the analytical result is as follows:

$$\begin{aligned} v_\perp &= v_\perp(0)e^{-i\Omega_0 t} - v_A\frac{\sum_k \Omega_k}{\Omega_0}e^{-ik(v_A t - z)-i\varphi_k} + v_A\frac{\sum_k \Omega_k}{\Omega_0}e^{i(kz(0)-\varphi_k)}e^{-i\Omega_0 t} \\ &= v_\perp(0)e^{-i\Omega_0 t} - v_A\frac{\sum_k B_k}{B_0}e^{-ik(v_A t - z)-i\varphi_k} + v_A\frac{\sum_k B_k}{B_0}e^{i(kz(0)-\varphi_k)}e^{-i\Omega_0 t} \end{aligned} \quad (34)$$

The relationships below between the temperature and velocity of protons are based on plasma which consists of an ensemble of protons,

$$T_\perp(t) = \frac{1}{2}\sum_{i=1}^{N}\frac{m_i v_\perp^2(t)}{N}; \quad T_\parallel(t) = \sum_{i=1}^{N}\frac{m_i v_\parallel^2(t)}{N} \quad (35)$$

where $T_\perp$ is the perpendicular kinetic temperature, $T_\parallel$ is the parallel kinetic temperature and N is total number of the protons.

We present the simulation results using test-particle calculations that build upon previous works [28, 30, 32, 33]. The test-particle simulation will be valid in partially ionized plasmas when no damping occurs. We discretize the Alfvén wave number by $k_j = k_{min} + (j-1)\frac{k_{max}-k_{min}}{J-1}$, for $j = 1, ..., J$, where $k_{min} = k_1 = 1 \times 10^{-8}\Omega_0/v_A$ and $k_{max} = k_J = 5 \times 10^{-8}\Omega_0/v_A$. This range of wave numbers implies that we are considering $1 \times 10^{-8}\Omega_0 < \omega < 5 \times 10^{-8}\Omega_0$, so that the wave frequencies are much lower than the proton gyrofrequency and also will be low enough to guarantee that no damping occurs [42]. The amplitude of each wave mode is considered to be constant, here we set $\delta B_w^2/B_0^2 = \zeta = 0.05$. The total number of test particles is 10^5, which are randomly distributed during the time interval $\Omega_0 t = [0, 2\pi]$ and along the spatial range $z\Omega_0/v_A = [0, 3 \times 10^9]$. As discussed earlier in this chapter, the relationship between the ion-neutral collision frequency and ion gyrofrequency is $\nu_{in} = a\Omega_0$. In this chapter, we vary the ratio a between 0.1 and 0.5, which is well within the acceptable range for describing the solar chromosphere as determined by Vernazza *et al.* [45]. The initial ion velocities are assumed to have a Maxwellian

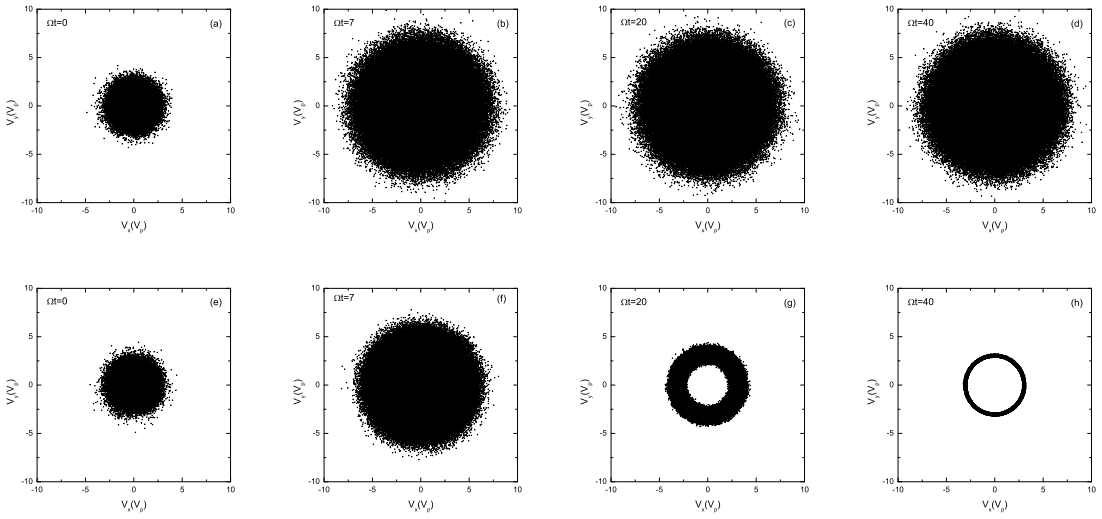

Figure 4: Velocity scatter plots of the test particles in the $v_x - v_y$ space in the case $\nu_{in} = 0$ (first line) and $\nu_{in} = 0.1\Omega_0$ (second line) at time $\Omega t = 0$, $\Omega t = 7$, $\Omega t = 20$ and $\Omega t = 40$, for input parameters $(\delta {B_w}^2/{B_0}^2, v_p/v_A) = (0.05,\ 0.07)$.

distribution with thermal speed v_p, which is less than v_A to ensure that the cyclotron resonance condition cannot be satisfied.

In Fig.4 we present scatter plots in the $v_x - v_y$ space which illustrate the process of particle heating. Here, the velocity is normalized to the initial thermal speed v_p, which is set to be $v_p = 0.07 v_A$. We compare nonresonant heating without and with neutral collisions in Fig.4. The results for the non-collisional case, where $a = 0$, shown in Fig.4 (a), (b), (c), and (d), are in accordance with the former results [30]. We find that collisional effects reduce the amount of heating over time and are responsible for creating a ring distribution. Since $\mathbf{u}(t) \approx 0$ is valid during the relatively short time scales considered in this chapter as explained above, a balance is reached between energy gained via Alfvén wave interactions and lost from collisions with cold neutrals. Thus the velocity distribution evolves into a "thin" ring structure, with all of the ions evolving to a single speed. This result can also be analytically approximated, and will be discussed in detail in the following paragraphs.

Fig.5 shows the temporal evolution of the kinetic temperatures, where the results

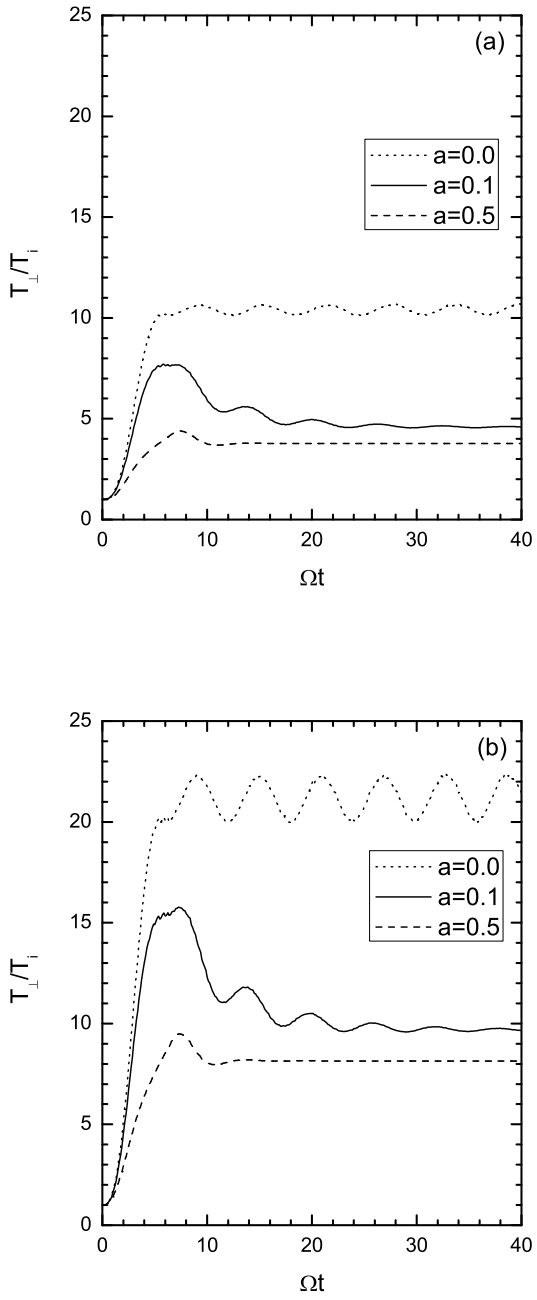

Figure 5: The temporal evolution of the perpendicular kinetic temperatures normalized with respect to their initial values T_i. The various input parameters, $(\delta {B_w}^2/{B_0}^2, v_p/v_A)$=(0.05, 0.07) and (0.12, 0.07) are shown in Fig.5(a) and Fig.5(b), respectively.

are based on two sets of input parameters $(\delta {B_w}^2/{B_0}^2, v_p/v_A)$=(0.05, 0.07) and (0.12, 0.07). The cases $a = 0$, 0.1 and 0.5 are represented by the dotted line, the solid line and the dashed line, respectively. The results again demonstrate that heating via nonresonant Alfvén wave interactions is possible, and that even in the presence of neutrals heating still occurs and reaches a steady value. We find the ratio of the ion-neutral collision frequency to the ion gyrofrequency, a, will directly affect the heating process. When the ratio a is larger, the heating process becomes less efficient. However, the low-beta plasmas are still significantly heated, as indicated in Fig.5 where the temperature $T_\perp(t)$ is much larger than the initial temperature T_i. This phenomenon may provide a partial explanation as to why the temperature of the chromosphere is higher than the photosphere while lower than the corona, as the fraction of ionized particles increases from the photosphere through the chromosphere and to the corona [45]. Furthermore, we can see from the evolution of the population in Fig.4 (e), (f), (g), and (h) that there exists a dynamic equilibrium between the heating and cooling of the ions, which is reached after a period of time. This is also demonstrated by the oscillations in temperature which decrease over time as shown in Fig.5 for the cases $a \neq 0$.

The results of the test particle calculations are strongly consistent with our analytical predictions. The ratio of frequencies a in the analytic solution Eq.(51) is in the term $e^{-\nu_{in}t}$ where $\nu_{in} = a\Omega_0$, thus $e^{-\nu_{in}t} = e^{-a\Omega_0 t}$. Hence, a larger value of a will result in a lower value of $e^{-\nu_{in}t}$, which will affect the value of ion kinetic temperatures as shown in Fig.5. Given the parameters $u(t) \approx 0$, $v_p = 0.07 v_A$, $\delta B_w^2/B_0^2 = \zeta = 0.05$, $a = 0.1$ and $t = 40$, the solution of Eq.(51) can be reduced to

$$\begin{aligned} |v_\perp| &\approx \left| -\frac{\sum_k \Omega_k \left[v_A - v_\parallel(0)\right](\Omega_0 + i\nu_{in})}{{\Omega_0}^2 + {\nu_{in}}^2} e^{-ik(v_A t - z) - i\varphi_k} \right| \\ &\approx \left| \frac{\sqrt{\zeta}\left[v_A - v_\parallel(0)\right](1 + ia)}{1 + a^2} e^{-ik(v_A t - z) - i\varphi_k} \right| \\ &\approx \sqrt{\zeta} \times v_A \left| (1 + ia) e^{-ik(v_A t - z) - i\varphi_k} \right| \approx \sqrt{\zeta} \times v_A \sqrt{1 + a^2} \approx 3.2 v_p \end{aligned} \quad (36)$$

where we use the approximations $e^{-\varepsilon} \approx 0$ when $\varepsilon > 3$, $|v_A - v_\parallel(0)| \approx |v_A|$ and $1 + a^2 = 1.01 \approx 1$. Thus after a period of time, the stable value of velocity is $3.2v_p$ which is in accordance with the ring structure of velocity distribution shown in Fig.4(h).

The physical mechanism of this heating can be described as follows: initially, the average ion velocity is zero, then ions are rapidly picked up by the Alfvén waves primarily in the transverse direction. Hence, the ions obtain an average perpendicular velocity. The parallel thermal motions of ions at a given location produce phase differences (randomization) between ions resulting in heating of the ion population. Due to the fact that the neutrals are given an approximately invariable bulk velocity, the heated ions will lose energy from ion-neutral elastic collisions throughout the process. This leads to an overall reduced efficiency of the ion heating relative to the simulation with no ion-neutral collisions.

CHAPTER III

PROTON HEATING VIA NONRESONANT INTERACTIONS WITH OBLIQUELY PROPAGATING ALFVÉN WAVES

We consider that the Alfvén waves have a spectrum, and that the dispersion relation can be described as $\omega = kv_A \cos\theta$ (v_A is the Alfvén speed, ω and k are the wave angular frequency and wave number, respectively; θ is the angle between the background magnetic field and Alfvén waves propagation). Without loss of generality, we consider left-hand circular polarization in this paper. The wave magnetic field vector $\delta\mathbf{B}_w$ and electric field vector $\delta\mathbf{E}_w$ can be expressed as

$$\delta\mathbf{B}_w = \sum_k B_k(\cos\theta\cos\phi_k\mathbf{i}_x - \sin\phi_k\mathbf{i}_y - \sin\theta\cos\phi_k\mathbf{i}_z), \tag{37}$$

$$\delta\mathbf{E}_w = -\frac{v_A}{c}(\cos\theta\mathbf{i}_z + \sin\theta\mathbf{i}_x) \times \delta\mathbf{B}_w \tag{38}$$

where $\mathbf{i}_x$, $\mathbf{i}_y$ and $\mathbf{i}_z$ are unit directional vectors, $\phi_k = k(v_A\cos\theta t - z\cos\theta - x\sin\theta) + \varphi_k$ denotes the wave phase and φ_k is the random phase for mode k. In the following, we pay attention to the protons only, whose equation of motion is described by

$$m_i\frac{d\mathbf{v}}{dt} = q_i\left(\delta\mathbf{E}_w + \frac{\mathbf{v}}{c}\times(\mathbf{B}_0 + \delta\mathbf{B}_w)\right), \quad \frac{d\mathbf{r}}{dt} = \mathbf{v} \tag{39}$$

where $\mathbf{v}$ is the ion velocity. Substituting Eq.(37) and Eq.(38) into Eq.(39) for $\delta\mathbf{B}_w$ and $\delta\mathbf{E}_w$, we get

$$\begin{aligned}\frac{m_i}{q_i}\frac{d\mathbf{v}}{dt} &= -\frac{v_A}{c}(\cos\theta\mathbf{i}_z + \sin\theta\mathbf{i}_x) \times \sum_k B_k(\cos\theta\cos\phi_k\mathbf{i}_x - \sin\phi_k\mathbf{i}_y - \sin\theta\cos\phi_k\mathbf{i}_z) \\ &+ \frac{\mathbf{v}}{c}\times(\mathbf{B}_0 + \sum_k B_k(\cos\theta\cos\phi_k\mathbf{i}_x - \sin\phi_k\mathbf{i}_y - \sin\theta\cos\phi_k\mathbf{i}_z)),\end{aligned} \tag{40}$$

After several steps of calculations, we get three components of Eq.(40) as follows:

$$\frac{dv_x}{dt} = -v_A \sum_k \Omega_k \cos\theta \sin\phi_k + \Omega_0 v_y - v_y \sum_k \Omega_k \sin\theta \cos\phi_k + v_z \sum_k \Omega_k \sin\phi_k \quad (41)$$

$$\frac{dv_y}{dt} = -v_A \sum_k \Omega_k \cos\phi_k + v_z \sum_k \Omega_k \cos\theta \cos\phi_k - v_x \Omega_0 + v_x \sum_k \Omega_k \sin\theta \cos\phi_k \quad (42)$$

$$\frac{dv_z}{dt} = v_A \sum_k \Omega_k \sin\theta \sin\phi_k - v_x \sum_k \Omega_k \sin\phi_k - v_y \sum_k \Omega_k \cos\theta \cos\phi_k \quad (43)$$

where $\Omega_0 = \frac{q_i B_0}{m_i c}$ (the proton gyrofrequency), $\Omega_k = \frac{q_i B_k}{m_i c}$. Normalizing the above equations (using time: Ωt, velocity: v_A, space: $x\Omega/v_A$, $z\Omega/v_A$), we get:

$$\begin{aligned}\frac{dv_x}{dt} &= -\frac{\sum_k B_k}{B_0} \cos\theta \sin\left[k(\cos\theta t - (z(0) + v_z t)\cos\theta - (x(0) + v_x t)\sin\theta) + \varphi_k\right] \\ &+ v_y - v_y \frac{\sum_k B_k}{B_0} \sin\theta \cos\left[k(\cos\theta t - (z(0) + v_z t)\cos\theta - (x(0) + v_x t)\sin\theta) + \varphi_k\right] \\ &+ v_z \frac{\sum_k B_k}{B_0} \sin\left[k(\cos\theta t - (z(0) + v_z t)\cos\theta - (x(0) + v_x t)\sin\theta) + \varphi_k\right] \quad (44)\end{aligned}$$

$$\begin{aligned}\frac{dv_y}{dt} &= -\frac{\sum_k B_k}{B_0} \cos\left[k(\cos\theta t - (z(0) + v_z t)\cos\theta - (x(0) + v_x t)\sin\theta) + \varphi_k\right] - v_x \\ &+ v_z \frac{\sum_k B_k}{B_0} \cos\theta \cos\left[k(\cos\theta t - (z(0) + v_z t)\cos\theta - (x(0) + v_x t)\sin\theta) + \varphi_k\right] \\ &+ v_x \frac{\sum_k B_k}{B_0} \sin\theta \cos\left[k(\cos\theta t - (z(0) + v_z t)\cos\theta - (x(0) + v_x t)\sin\theta) + \varphi_k\right] \quad (45)\end{aligned}$$

$$\begin{aligned}\frac{dv_z}{dt} &= \frac{\sum_k B_k}{B_0} \sin\theta \sin\left[k(\cos\theta t - (z(0) + v_z t)\cos\theta - (x(0) + v_x t)\sin\theta) + \varphi_k\right] \\ &- v_x \frac{\sum_k B_k}{B_0} \sin\left[k(\cos\theta t - (z(0) + v_z t)\cos\theta - (x(0) + v_x t)\sin\theta) + \varphi_k\right] \\ &- v_y \frac{\sum_k B_k}{B_0} \cos\theta \cos\left[k(\cos\theta t - (z(0) + v_z t)\cos\theta - (x(0) + v_x t)\sin\theta) + \varphi_k\right] \quad (46)\end{aligned}$$

3.1 SMALL ANGLE APPROXIMATION ($\sin\theta \approx \theta$)

We first analytically study the situation with small angle θ ($0^o \sim 5^o$) which results in the reasonable approximation $\sin\theta \approx \theta$. Then Eqs.(37,38) are reduced to

$$\delta\mathbf{B}_w = \sum_k B_k(\cos\phi_k \mathbf{i}_x - \sin\phi_k \mathbf{i}_y - \theta\cos\phi_k \mathbf{i}_z), \quad (47)$$

$$\delta\mathbf{E}_w = -\frac{v_A}{c}(\mathbf{i}_z + \theta\mathbf{i}_x) \times \delta\mathbf{B}_w \tag{48}$$

which are in accordance with the expressions in previous works [30, 32]. Substituting Eqs.(47,48) into Eq.(39) for $\delta\mathbf{B}_w$ and $\delta\mathbf{E}_w$, defining $v_\perp = v_x + iv_y$, $v_\parallel = v_z$, and $\delta B_\omega = \sum_k B_k e^{-i\phi_k}$; we are left with

$$\frac{dv_\perp}{dt} + i(\Omega_0 - \sum_k \Omega_k\theta\cos\phi_k)v_\perp = i(v_\parallel - v_A)\sum_k \Omega_k e^{-i\phi_k} \tag{49}$$

$$\frac{dv_\parallel}{dt} = \sum_k \Omega_k(v_A\theta\sin\phi_k - v_x\sin\phi_k - v_y\cos\phi_k), \quad \frac{dz}{dt} = v_\parallel \tag{50}$$

We assume $v_\parallel \approx v_\parallel(0)$, where $v_\parallel(0)$ is the particles initial parallel velocity. The approximation is valid only when θ is small, $\sum_k \frac{\Omega_k}{\Omega_0} = \sum_k \frac{B_k}{B_0}$ is small enough, and the frequencies of the Alfvén wave are sufficiently low to ensure that $\mid \Omega_0 \mid \gg \mid k\left(v_\parallel(0) - v_A\right) \mid$. In this section, we focus on the perpendicular velocity component due to the fact that the ions temperature increase is more prominent along the perpendicular direction than the parallel direction when Alfvén wave propagating is along the ambient magnetic filed direction [30, 32], thus the results should be appropriate for the very small θ case. With the initial condition $v_\perp = v_\perp(0)$ and $z = z(0)$, the solution of Eq.(49) can be written as:

$$\begin{aligned} v_\perp &= v_\perp(0)e^{-i\Omega_0 t + \frac{i\sum_k \Omega_k\theta}{kv_A}[\sin(kv_A t - kz + \varphi_k) + \sin(kz(0) - \varphi_k)]} - v_A\frac{\sum_k B_k}{B_0}e^{-ik(v_A t - z) - i\varphi_k} \\ &+ v_A\frac{\sum_k B_k}{B_0}e^{ikz(0) - i\varphi_k}e^{-i\Omega_0 t + \frac{i\sum_k \Omega_k\theta}{kv_A}[\sin(kv_A t - kz + \varphi_k) + \sin(kz(0) - \varphi_k)]} \end{aligned} \tag{51}$$

where we use the approximation that $\Omega_0 - k[v_A - v_\parallel(0)] \approx \Omega_0$ and $z = z(0) + v_\parallel(0)t$.

The above result is applicable to a single proton. The relationships below between the temperature and velocity of protons are based on plasma which consists of an ensemble of protons,

$$T_\perp(t) = \frac{1}{2}\sum_{i=1}^{N}\frac{m_i v_\perp^2(t)}{N}; \quad T_\parallel(t) = \sum_{i=1}^{N}\frac{m_i v_\parallel^2(t)}{N}$$

where $T_\perp$ is the perpendicular kinetic temperature, $T_\parallel$ is the parallel kinetic temperature and N is total number of the protons.

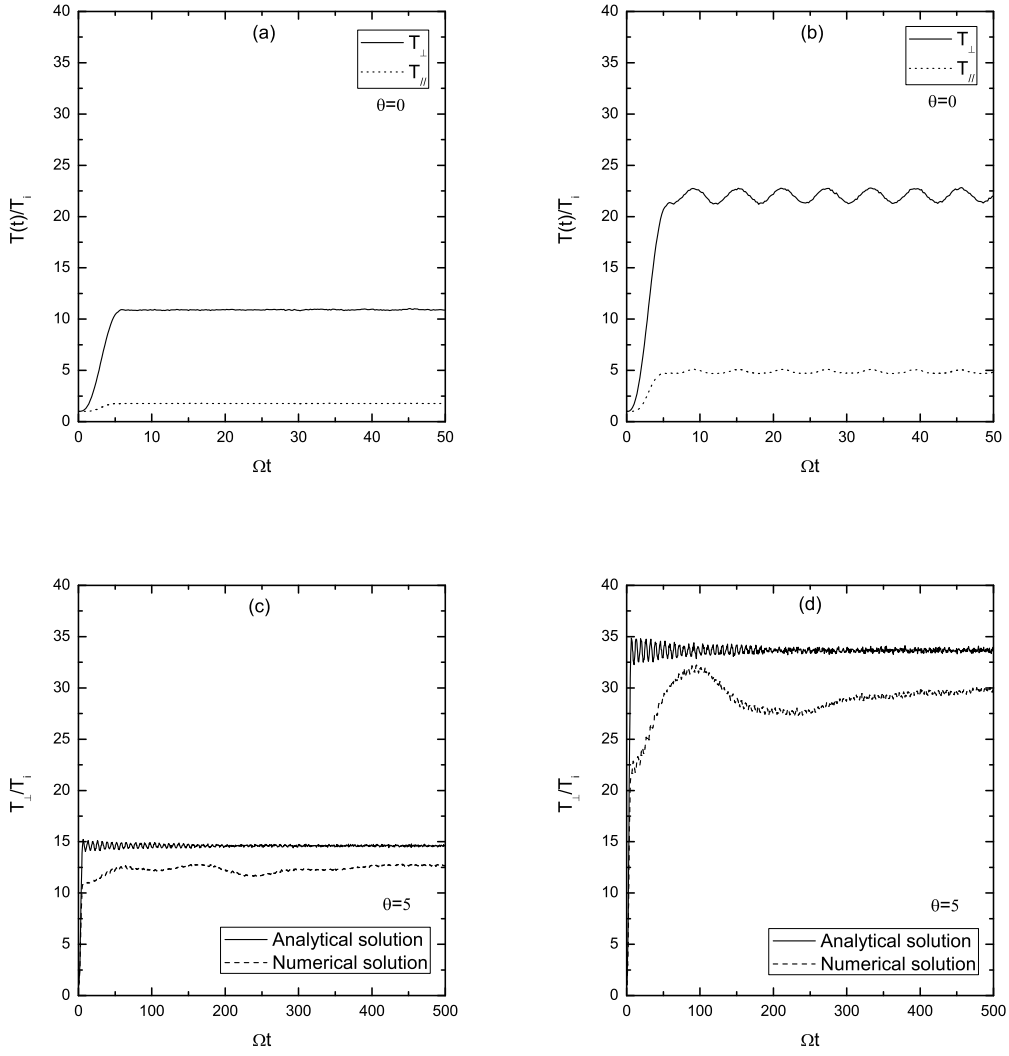

Figure 6: The temporal evolution of the perpendicular (parallel) kinetic temperatures normalized with respect to their initial values T_i. The various input parameters $(\delta {B_w}^2/{B_0}^2, v_p/v_A, \theta)$: (a) (0.05, 0.07, 0^o), (b) (0.12, 0.07, 0^o), (c) (0.05, 0.07, 5^o) and (d) (0.12, 0.07, 5^o).

We compare the results of analytic solution with the simulation results using test-particle calculations that build upon previous works [28, 30, 32, 33]. We discretize the Alfvén wave number by $k_j = k_{min} + (j-1)\frac{k_{max}-k_{min}}{J-1}$, for $j = 1, ..., J$, where $k_{min} = k_1 = 1 \times 10^{-2}\Omega_0/v_A$ and $k_{max} = k_J = 5 \times 10^{-2}\Omega_0/v_A$. This range of wave numbers implies that we are considering $1 \times 10^{-2}\Omega_0 < \omega < 5 \times 10^{-2}\Omega_0$, so that the wave frequencies are much lower than the proton gyrofrequency. The amplitude of each wave mode is considered to be constant. Here we set $\delta B_w^2/B_0^2 \sim 0.05$ and 0.12. The total number of test particles is 10^5, which are randomly distributed during the time interval $\Omega_0 t = [0, 2\pi]$ and in the spatial area $z\Omega_0/v_A \otimes x\Omega_0/v_A = [0, 3 \times 10^3] \otimes [0, 3 \times 10^3]$. The initial ion velocities are assumed to have a Maxwellian distribution with thermal speed v_p=0.07v_A, which is less than v_A to ensure that the cyclotron resonance condition cannot be satisfied.

The results in Fig.6(a)&(b) are based on the test particle simulation when $\theta = 0$. The perpendicular and parallel kinetic temperature are represented by the solid line and the dotted line, respectively. Fig.6(a)&(b) show our simulation results are consistent with the results shown in previous work [30]. In Fig.6(c)&(d), the analytic and numerical results for $\theta = 5^o$ are represented by the solid line and the dashed line, respectively. Fig.6(c)&(d) compare the analytic and numerical solution for $T_\perp$, which shows that the results are accordance with each other. Fig.6(c)&(d) show us that the kinetic temperature of the analytic solution is always higher than that of the numerical simulation, which primarily results from the approximation of $\Omega_0 - k[v_A - v_\parallel(0)] \approx \Omega_0$. From Fig.6, one can see that the kinetic temperature with angle $\theta = 5^o$ is a litter higher than the temperature with angle $\theta = 0^o$, which is caused by the oblique effect (the existence of angle θ).

3.2 LARGE ANGLE SIMULATIONS

In Fig.7 we present scatter plots in the $v_x - v_y - v_z$ space, which illustrate the process of particle heating. Here, the velocity is normalized to the initial thermal speed v_p. The input parameters are shown in the caption of the figure. We compare nonresonant heating without and with angle θ in Fig.7. The results for $\theta = 0$, shown in the first row of Fig.7, are in accordance with the former results [30]. The rest of Fig.7 demonstrates the effect of angle θ, $\delta {B_w}^2/{B_0}^2$, and time steps on the velocity distribution of ions. Additionally, one finds that when $\theta \neq 0$, $v_\parallel$ becomes larger than $v_\perp$, which means $v_\parallel$ are greatly accelerated during the pickup process while $v_\parallel$ increase only a little under the situation with $\theta = 0$. It also indicates that $T_\parallel$ can become greater than $T_\perp$, which is different from the results shown in the previous works [30, 32, 33].

Figs.8 and 9 show the temporal evolution of the kinetic temperatures, where the results are based on the input parameters $(\delta {B_w}^2/{B_0}^2, v_p/v_A)$=(0.05, 0.07) and (0.12, 0.07) with different angles θ. The parallel and perpendicular kinetic temperature are represented by the dashed line and the solid line, respectively. The second row of Figs.8 and 9 independently show the perpendicular kinetic temperature since the large difference in scale would make them difficult to compare on the same figure. The results again demonstrate that heating via nonresonant Alfvén wave interactions is possible. We find the parallel kinetic temperature becomes much larger than perpendicular component when $\theta \neq 0$. Also, the larger the angle θ, the more significant difference between $T_\parallel$ and $T_\perp$ for the heated ions. The low-beta plasmas are significantly heated, as indicated in Figs.8 and 9 where both $T_\perp(t)$ and $T_\parallel(t)$ are much larger than the initial temperature T_i, especially when θ is large. This phenomenon may provide a partial quantized explanation as to why the temperature of the corona is higher than the photosphere and chromosphere. The reason for $T_\parallel$ becoming larger than $T_\perp$ can be briefly explained as follows.

From Eqs.(44-46), we know that each velocity component is coupled with each

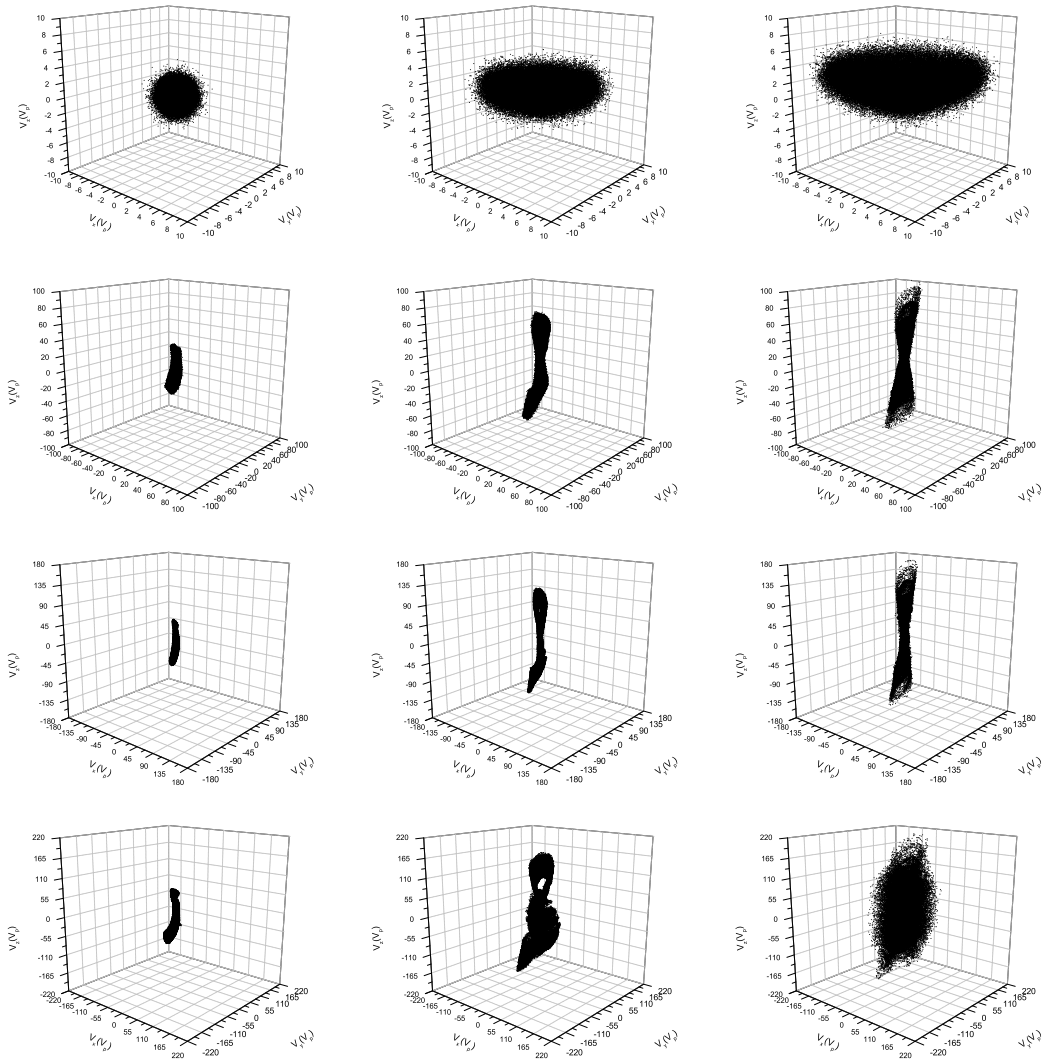

Figure 7: Velocity scatter plots of the test particles in the $v_x - v_y - v_z$ space in the case (first line) $\theta = 0$ for input parameters $(\delta {B_w}^2/{B_0}^2, v_p/v_A,\, \theta,\, \mathrm{t}) = (0.05,\, 0.07,\, 0^o,\, 0)$, $(0.05,\, 0.07,\, 0^o,\, 20)$, $(0.12,\, 0.07,\, 0^o,\, 20)$; (second line) $\theta = \pi/6$ for input parameters $(\delta {B_w}^2/{B_0}^2, v_p/v_A,\, \theta,\, \mathrm{t}) = (0.05,\, 0.07,\, 30^o,\, 20)$, $(0.05,\, 0.07,\, 30^o,\, 50)$, and $(0.05,\, 0.07,\, 30^o,\, 400)$; (third line) $\theta = \pi/3$ for input parameters $(\delta {B_w}^2/{B_0}^2, v_p/v_A,\, \theta,\, \mathrm{t}) = (0.05,\, 0.07,\, 60^o,\, 20)$, $(0.05,\, 0.07,\, 60^o,\, 50)$, and $(0.05,\, 0.07,\, 60^o,\, 400)$; (fourth line) $\theta = \pi/3$ for input parameters $(\delta {B_w}^2/{B_0}^2, v_p/v_A,\, \theta,\, \mathrm{t}) = (0.12,\, 0.07,\, 60^o,\, 20)$, $(0.12,\, 0.07,\, 60^o,\, 50)$, and $(0.12,\, 0.07,\, 60^o,\, 400)$.

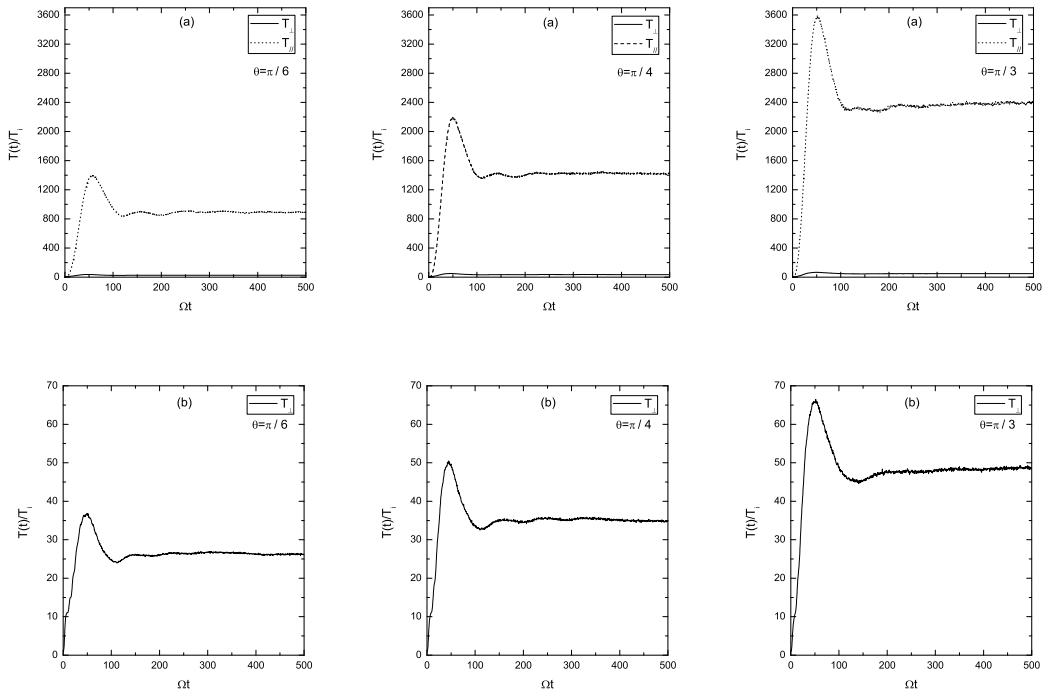

Figure 8: The temporal evolution of the parallel and perpendicular kinetic temperatures normalized with respect to their initial values T_i. For input parameters (first column) $(\delta {B_w}^2/{B_0}^2, v_p/v_A, \theta) = (0.05, 0.07, \pi/6)$; (second column) $(\delta {B_w}^2/{B_0}^2, v_p/v_A, \theta) = (0.05, 0.07, \pi/4)$; (third column) $(\delta {B_w}^2/{B_0}^2, v_p/v_A, \theta) = (0.05, 0.07, \pi/3)$.

other. Since Alfvén waves propagating obliquely to the ambient magnetic field, the magnetic turbulence in z direction makes contributions to accelerating v_z. Once v_z increases, v_x and v_y will also increase according to Eqs.(44-45) since the terms contain v_z are positive in Eq.(44-45). However, as indicated by Eq.(46), the increase of v_x and v_y will decrease v_z since the terms contain v_x and v_y are negative in Eq.(46). Though the terms contain v_z in Eq.(44-45) will decrease, the term contain v_z are still much larger than the rest terms in Eqs.(44-45), thus v_x and v_y can still increase until the final equilibrium state are reached. Hence, there exists a dynamic equilibrium process before they get the final stable values. Finally, we have to mention that this section is still under work. We will try to find if the time steps are long enough, and what will happen to the evolution of both ion velocity distribution and kinetic temperature.

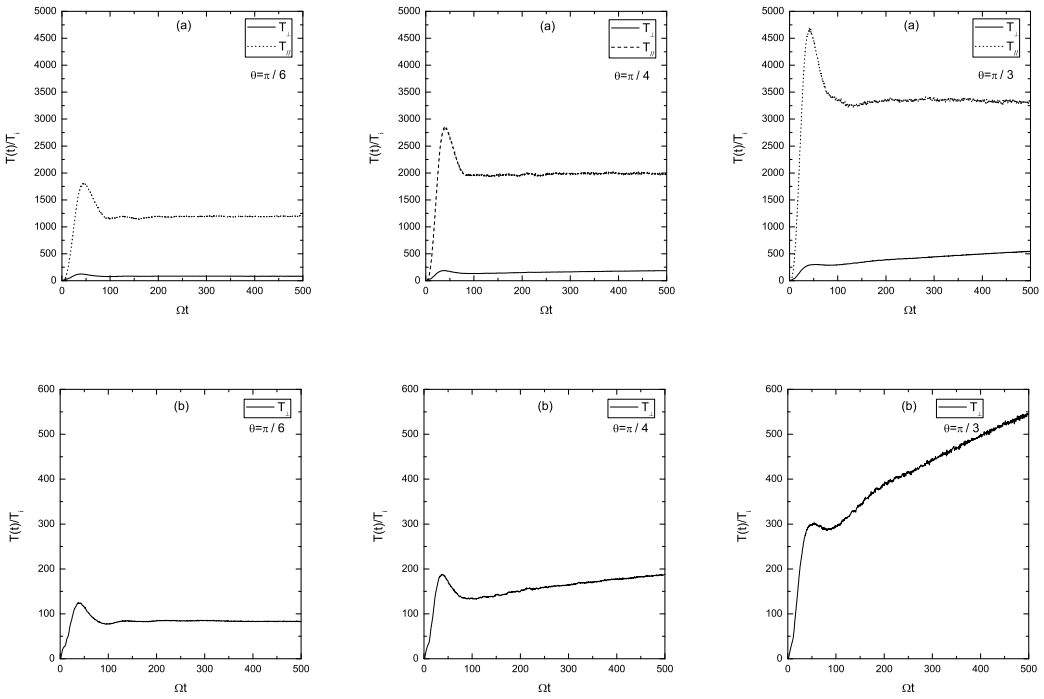

Figure 9: The temporal evolution of the parallel and perpendicular kinetic temperatures normalized with respect to their initial values T_i. For input parameters (first column) $(\delta {B_w}^2/{B_0}^2, v_p/v_A, \theta) = (0.12, 0.07, \pi/6)$; (second column) $(\delta {B_w}^2/{B_0}^2, v_p/v_A, \theta) = (0.12, 0.07, \pi/4)$; (third column) $(\delta {B_w}^2/{B_0}^2, v_p/v_A, \theta) = (0.12, 0.07, \pi/3)$.

CHAPTER IV

CONCLUSION

In summary, we show that partially ionized low beta plasmas can be heated by a spectrum of low-frequency Alfvén waves with large amplitude, which have been observed in the chromosphere [13]. We also show that ions can be picked up by obliquely propagating low-frequency Alfvén waves with large amplitude in fully ionized low-beta plasmas. These are contrary to the linear theory, according to which ions can only be heated through resonant interactions with Alfvén waves. In our model, the frequencies of the Alfvén waves are much lower than the ion cyclotron frequency, so the cyclotron resonant condition is not met. This also ensures that the waves will not be damped by ion-neutral collisions [42]. For heating of ions in partially ionized plasmas, we find that the amount of heating depends on the ratio a, where less heating occurs when more collisions are taken into account. However, in all cases, significant heating of the ions occurred. Furthermore, we show that the velocity distribution will form a ring structure during the heating process when elastic ion-neutral collisions are considered, which is consistent with our analytic approximation. Our results demonstrate significant heating of ions through nonresonant Alfvén wave interactions in partially ionized plasmas, which may provide an alternate source of heating in the solar chromosphere than previously considered. For ion heating via nonresonant interactions with obliquely propagating Alfvén waves in fully ionized plasmas, we find the parallel kinetic temperature can become even greater than the perpendicular component which is different from the results shown in previous work [30,32,33]. The larger the angle θ is, the more heated the ions become. Also, the larger the angle θ, the more significant the difference between $T_{\parallel}$ and $T_{\perp}$ for the heated ions.

REFERENCES

[1] R. A. Garcia, et al., Science **316**, 1591C1593 (2007).

[2] S. Basu et al., Astrophys. J. **699**, 1403 (2009).

[3] Zirker, Jack B. (2002). *Journey from the Center of the Sun*. Princeton University Press. pp. 15C34. ISBN 9780691057811.

[4] "Nasa - Sun". Nasa.gov. 2007-11-29. Retrieved 2009-07-11. http://www.nasa.gov/worldbook/sun_worldbook.html.

[5] "NASA/Marshall Solar Physics". Solarscience.msfc.nasa.gov. 2007-01-18. http://solarscience.msfc.nasa.gov/interior.shtml. Retrieved 2009-07-11.

[6] The Sun - Introduction, http://imagine.gsfc.nasa.gov/docs/science/know_l1/sun.html.

[7] "SP-402 A New Sun: The Solar Results From Skylab", http://history.nasa.gov/SP-402/p2.htm.

[8] E. G. Gibson, (1973). *The Quiet Sun*. NASA. ASIN B0006C7RS0.

[9] R. Erdelyi, I. Ballai, Astron. Nachr. **328**, 726C733 (2007).

[10] V. H. Hansteen, E. Leer, Astrophys. J. **482**, 498C509 (1997).

[11] A. G. Donald (1 June 2005). "Voyager Termination Shock". Department of Physics and Astronomy (University of Iowa). http://www-pw.physics.uiowa.edu/space-audio/voyager/termination-shock/. Retrieved 2008-02-06.

[12] T. J. M. Boyd, and J. J. Sanderson, *The Physics of Plasmas*, Cambridge University Press, 2003.

[13] B. De Pontieu, S. W. McIntosh, M. Carlsson et al., Science **318**, 1574 (2007).

[14] G. A. Gary, Sol. Phys. **203**, 71 (2001).

[15] J.W. Belcher, L. Davis, Jr., and E. J. Smith, J. Geophys. Res. **74**, 2302 (1969).

[16] F. M. Neubauer et al., Nature (London) 321, 352 (1986).

[17] B. Hanson and D. Voss, Science **318**, 1571 (2007).

[18] D. B. Jess, M. Mathioudakis, R. Erdelyi, P. J. Crockett, F. P. Keenan, D. J. Christian, Science **323**, 1582 (2009).

[19] A. K. Nekrasov, Nucl. Fusion. **10**,387 (1970).

[20] M. A. Lieberman and A. J. Lichtenberg, Plasma Phys. **15**, 125 (1973).

[21] J. V. Hollweg, Rev. Geophys. Space Phys. **16**, 689 (1978).

[22] H. Abe, H. Okada, R. Itatani, M. Ono, and H. Okuda, Phys. Rev. Lett. **53**, 1153 (1984).

[23] P. A. Isenberg, and J. V. Hollweg, J. Geophys. Res. **88**, 3923 (1983).

[24] S. R. Cranmer, G. B. Field, and J. L. Kohl, Astrophys. J. **518**, 937 (1999).

[25] W. I. Axford et al., Space Sci. Rev. **87**, 25 (1999).

[26] C. Y. Tu, and E. Marsch, J. Geophys. Res. **106**, 8233 (2001).

[27] Y. Li, Peter H. Yoon, C. S. Wu, A. T. Weatherwax, J. K. Chao, and B. H. Wu, Phys. Plasmas **4**, 11 (1997).

[28] C. S. Wu, Peter H. Yoon, and J. K. Chao, Phys. Plasmas **4**, 856 (1997).

[29] L. Chen, Z. H. Lin, and R. White, Phys. Plasmas **8**, 4713 (2001).

[30] C. B. Wang, C. S. Wu, and P.H. Yoon, Phys. Rev. Lett. **96**, 125001 (2006).

[31] C. S. Wu, and P.H. Yoon, Phys. Rev. Lett. **99**, 075001 (2007).

[32] Q. M. Lu, and X. Li, Phys. Plasmas **14**, 042303 (2007).

[33] X. Li, Q. M. Lu, and B. Li, Astrophys. Lett. **661**, L105 (2007).

[34] S. Bourouaine, E. Marsch, and C. Vocks, Astrophys. Lett. **684**, L119 (2008).

[35] J. A. Araneda, E. Marsch, and A. F. -Viñas, Phys. Rev. Lett. **100**, 125003 (2008).

[36] J. A. Araneda, Y. Maneva, and E. Marsch, Phys. Rev. Lett. **102**, 175001 (2009).

[37] C. F. Dong, C. S. Paty, Heating of ions by low-frequency Alfvén waves in partially inoized plasmas, submitted.

[38] C. F. Dong, C. S. Paty, Proton heating via nonresonant interactions with obliquely propagating Alfvén waves, in preparation.

[39] D. A. Gates, N. N. Gorelenkov, and R. B. White, Phys. Rev. Lett. **87**, 205003 (2001).

[40] Fredrickson, E. D., et al., Phys. Plasmas **9**, 2069 (2002).

[41] Y. Zhang et al., Phys. Plasmas **15**, 012103 (2008).

[42] J. E. Leake, T. D. Arber, and M. L. Khodachenko, Astron. Astrophys. **442**, 1091 (2005).

[43] B. De Pontieu and G. Haerendel, Astron. Astrophys. **338**, 729 (1998).

[44] B. De Pontieu, P. C. H. Martens and H. S. Hudson, Astrophys. J. **558**, 859 (2001).

[45] J. E. Vernazza, E. H. Avrett, and R. Loeser, ApJS **45**, 635 (1981).